Numerical examination of exergy performance of a hybrid solar system equipped with a sheet-and-sinusoidal tube collector: Developing a predictive function using artificial neural network

Chuan Sun [a,b], Mohammad N. Fares [c], S. Mohammad Sajadi [d], Z. Li [e,f,**], Dheyaa J. Jasim [g], Karrar A. Hammoodi [h], Navid Nasajpour-Esfahani [i], Soheil Salahshour [j,k,l], As'ad Alizadeh [m,*]

[a] School of Electromechanical and Intelligent Manufacturing, Huanggang Normal University, Huanggang, China
[b] Bosen Ruijie New Energy Technology (Hubei) Co., Ltd, Huanggang, China
[c] Department of Chemical Engineering, Faculty of Engineering, University of Basrah, Basrah, Iraq
[d] Department of Nutrition, Cihan University-Erbil, Kurdistan Region, Iraq
[e] Donghai Laboratory, Zhoushan Zhejiang 316021, China
[f] Faculty of Mechanical Engineering, Opole University of Technology, Opole, 45-758, Poland
[g] Department of Petroleum Engineering, Al-Amarah University College, Maysan, Iraq
[h] Department of Air Conditioning and Refrigeration, Faculty of Engineering, University of Warith Al-Anbiyaa, Karbala, 56001, Iraq
[i] Department of Material Science and Engineering, Georgia Institute of Technology, Atlanta, 30332, USA
[j] Faculty of Engineering and Natural Sciences, Istanbul Okan University, Istanbul, Turkey
[k] Faculty of Engineering and Natural Sciences, Bahcesehir University, Istanbul, Turkey
[l] Department of Computer Science and Mathematics, Lebanese American University, Beirut, Lebanon
[m] Department of Mechanical Engineering, College of Engineering, Urmia University, Urmia, Iran

ARTICLE INFO

ABSTRACT

Integrating cooling systems with photovoltaic-thermal (PVT) collectors has the potential to mitigate the exergy consumption in the building sector due to their capability for simultaneous power and thermal energy generation. The simultaneous utilization of nanofluid and geometry modification resulted in a synergetic enhancement in the performance of PVTs and thereby reducing their sizes and costs. In addition, there is still a lack of high accurate predictive model for the estimation of the performance of PVTs at a given Re number and nanofluid concentration ratio to be used in engineering design for the further product commercialization. To this end, the current numerical study investigates the exergy electricity, thermal, and overall exergies of a building-integrated photovoltaic thermal (BIPVT) solar collector with Al_2O_3/water coolant. The increase in nanoparticle concentration (ω) from 0 % to 1 % increased the useful thermal exergy and overall exergy efficiency ($Ex_{u,t}$/ Υ_{ov}) by 0.3999 %/0.0497 %, 1.3959 %/0.2598 %, and 0.7489 %/0.1771 % at Re numbers of 500, 1000, and 1500, respectively, while $Ex_{u,t}$/ Υ_{ov} exhibited a reducing trend at $Re = 2000$; 0.3928 %/0.1056 % decrease. In addition, the increase in ω from 0 % to 1 % caused the useful electricity and electrical exergy ($Ex_{u,e}$/ Υ_e) to be diminished by 0.0060 %/0.0025 % at Res 500 and 1000, and to be escalated by 0.0113 %/0.0055 % at Res of 1500 and 2000. Meanwhile, the Re augmentation, from 500 to 2000, improved the $Ex_{u,t}$, Ex_e, Υ_e, and Υ_{ov} by 60 %, 1.26 %, 1.26 %, and 17.50 %, respectively, at different ω s. In

---

* Corresponding author.
** Corresponding author.
E-mail addresses: z.li@po.edu.pl (Z. Li), asad.alizadeh2010@gmail.com (A. Alizadeh).

addition, two functions were developed and proposed by applying a group method of data handling-type neural network (GMDH-ANN) to forecast the value of Υ_{ov} based on two input values (Re and ω). The results showed high accuracy of the proposed model with MSE, EMSE, and R^2 of 0.0138, 0.1143, and 0.99785, respectively.

1. Introduction

The population growth, the need for energy, and fossil fuel consumption have led to escalating the Carbone emissions and the harmful effects of that on human life. Therefore, applying the technologies using which the energy could be produced with no greenhouse gas emissions seems to be the most important duty in the current era. Renewable energy sources, such as biomass, geothermal resources [1,2] , sunlight, water, and wind, are natural resources that can be converted into these types of energy. Also, using The building sector constitutes 30 % of the total energy consumption and 26 % of the total produced emissions. The building-integrated photovoltaic thermal (BIPVT) device could be installed either on the top of the building or its facades and generate part of the power and heating energy requirement of the building. This technology benefits the PV solar panel at the bottom of which a cooling absorber with a coolant fluid (air, water, or nanofluid) is designed to remove the thermal energy of the PV plate, reduce its temperature, and thereby enhance the PV electrical efficiency [3]. The thermal energy that is delivered to the cooling fluid is used as a thermal source of different HVAC instruments such as absorption chiller [4,5], heat pump [6–8], or even used for preparing domestic hot water [9]. It has been proven that solar energy (solar thermal or solar electricity) could be employed to supply a major part of energy requirements, particularly in regions with high radiation levels [10–12]. The efficient design of the solar thermal collectors brings their low costs and occupied installation space [13]. Since the absorber of BIPVT is kind of a heat exchanger, several techniques have been introduced and tested to enhance the performance of BIPVT such as using sinusoidal wavy channels, applying absorber tubes with fins, as well as utilizing different nanofluids (NFs) as the cooling medium. Employing both corrugated tubes and NFs simultaneously has received much attention due to its numerous applications. Several techniques are used in the heat exchangers to improve their hydrothermal performance and thereby reduce their sizes such as applying the ribbed tubes [14], twisted tubes [15], turbulator insert tubes [16], and corrugated tubes [17]. Wang et al. [18] experimentally investigated the effect of corrugated tubes and NF on the thermal performance of heat exchangers. They showed that the simultaneous use of TiO_2 NF with nanoparticle concentration of 0.5 % and corrugated tube leads to improving the heat transfer performance by 4.8–66.3 % over the heat exchanger with the plain tube and pure water. Although, the exergy efficiency of the corrugated tube is lower than that of the smooth tube. Wei et al. [19] conducted a numerical analysis to study the effect of corrugated helical tube and water/Al_2O_3 NF on the thermal efficiency of a coiled heat exchanger tube considering the constant temperature at the tube wall. In that study, four volume fractions between 0.01 and 0.04 as well as three particle sizes of 10, 20, and 30 nm were employed in calculations. The authors reported that the combined use of water/Al_2O_3 NF and corrugated helical tube leads to improving the heat transfer performance by 29 %. Also, the Nusselt number increased by 31 % with an increase in volume fraction. Islam et al. [20] conducted the numerical analysis of a hybrid NF in a rectangular corrugated tube for Re = 500–2000. Based on the outputs, the non-uniform and periodic corrugated wall tubes exhibited a higher thermal performance and pumping power as compared to the uniform corrugated tube. Meanwhile, the pumping power ratio and Nu number in the periodic corrugated tube with hybrid NF increased from 1.24 % to 1.36 % and 6.66 %–29.34 %, respectively, against the tube with the pure water. Zheng et al. [21] presented a procedure for heat transfer enhancement using a combined method of four different NFs and corrugated structures in a double-tube heat exchanger. According to the results, the SiC/water NF with a nanoparticle concentration of 1.5 % entails a 59 % increment in the thermal performance of the double tube heat exchanger. Qi et al. [22] performed the numerical and experimental analyzes to determine the impact of Re number and volume fraction of TiO_2 nanoparticles on the thermal performance of corrugated and circular steel tubes. The outcomes revealed that combined use of corrugated tube and TiO_2/water NF leads to a 53.95 % improvement in the heat transfer efficiency of the unit. Shahsavar et al. [23] conducted a three-dimensional numerical analysis to investigate the influence of NF and twisted tube on the hydrothermal performance of a heat exchanger. Different scenarios of the tube with the constant pitch ratio and variable pitch ratio were examined. The results showed that the variable pitch scenario exhibited the highest thermal performance and lowest entropy generation rate. In addition, the authors developed two predictive models for the energy and exergy performance of the system using an evolutionary machine learning method. Bahiraei et al. [24] numerically studied Al_2O_3/water NF flow and heat transfer in three corrugated tube and found that the heat transfer coefficient of the unit enhanced around 44.91 % by the volume fraction increment of 0.02. Shuvo et al. [25] performed a theoretical research and investigated the effect of water/Cu-Al_2O_3 hybrid NF on the heat transfer performance of a corrugated tube from the energy management point of view. The reported data from the authors indicated that the best heat transfer performance of the unit is related to a volume fraction of 2 %, corrugation height of 0.0318 D, and shear stress Re number of 314. Khan et al. [26] performed the numerical analysis of using a corrugated absorber tube in a parabolic trough solar thermal collector with hybrid NF of oil/MgO-MWCNT and considering the Re numbers of 3000–100000. The results were compared with the solar collector with the smooth tube. The finding demonstrated that the corrugated tube enhances the thermal efficiency of the solar thermal collector against the smooth absorber tube. In addition, 7.22 % increase in thermal efficiency was obtained as nanoparticle concentration increased from 0.25 % to 2 %. Ajeel et al. [27] carried out the numerical and experimental simulations of different NFs flow and heat transfer inside the corrugated pipes considering the Re number of 10,000 and nanoparticle volume fractions of 1 % and 2 %. The employed NFs were suspension of SiO_2 and Al_2O_3 in the pure water. According to the results, with an increase in volume fraction, the thermal performance and pressure drop are increased. Also, SiO_2 NF enhanced the thermal efficiency 1.94 times as compared to Al_2O_3 in a volume fraction of 2 %. Wang et al. [28] performed a numerical investigation on the heat transfer enhancement in a heat exchanger by
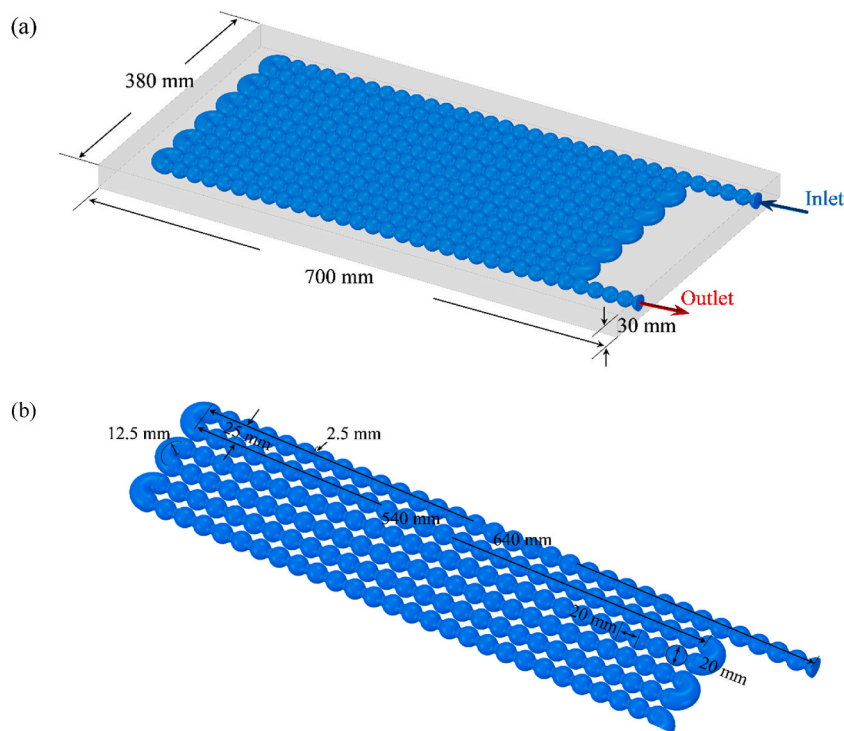
Fig. 1. Demonstrative sketches of the geometry.

applying Al_2O_3/CuO/water NF and twisted tape turbulator. The studied ranges of *Re* number and nanoparticle volume fraction were as 10000–20000 and 2–6%, respectively. Results indicated that the thermal efficiency of the system is improved by 126 % in *Re* number of 20000 and volume fraction of 6 %. Maddah et al. [29] added Al_2O_3/TiO_2/water NF and twisted tape inside a double tube heat exchanger and found that this combination exhibits the best exergy efficiency for the system. A compound use of TiO_2/water NF and rotating twisted tape inside a tube was experimentally evaluated by Qi et al. [30] to investigate the heat transfer performance and exergy efficiency of the unit. According to the author's results, a 101.6 % improvement was observed in heat transfer and exergy efficiency. An experimental work was done by Naphon [31] to investigate the flow and heat transfer feature of water/TiO_2 NF s in a spirally coiled tube. Based on the results, at the volume fraction of 0.05 %, a 34.07 % improvement in the *Nu* number was obtained over the case with pure water as working fluid. An experimental study was investigated by Zhai et al. [32] to determine the effectiveness of NFs and screw pitch on the heat transfer performance of a spiral tube. The results demonstrated that, the spiral tube with a screw pitch of 10 cm entails a 62 % increment in the heat transfer performance. Akbarzadeh et al. [33] simulated a numerical investigation in the corrugated tubes with Cu/water NF considering *Re* numbers 300 to 600, and volume fractions ranging from 0.01 to 0.05. The results showed that the *Nu* number is enhanced by about 56 % at *Re* = 600 and the volume fraction of 1 %. The impact of corrugated height and pitch on the heat transfer performance of a helical coiled tube was investigated by Darzi et al. [34] considering *Re* number ranging from 2000 to 8000 and Dean number ranging from 496 to 2806. The outcomes demonstrated that the higher corrugated height and the lower corrugated pitch entail a significant increment in thermal efficiency. The effect of employing a helical corrugated tube in a parabolic trough solar collector was assessed by Akbarzadeh and Valipour [35] from the energy and exergy points of view. The authors showed that the corrugated tubes entail the highest enhancement in the transitional regime. Esfahani and Languri [36] investigated the heat transfer characteristics of a shell-tube heat exchanger imbibed to the graphene oxide nano-sheets NF from the exergy efficiency point of view. Based on the best-reported result, the used NF leads to a decrease in the exergy loss up to 109 %. Chen et al. [37] accomplished new research by investigating the impact of using corrugation with different depths and pitches on the heat transfer performance of the heat exchanger from an exergy and economy points of view. They concluded that utilizing corrugated tubes could increase the *Nu* number up to 1.54 times. The combined use of Fe_3O_4/water NFs in a corrugated tube and the magnetic field was experimentally studied by Mei et al. [38]. Based on the findings, a 17.6 % improvement in the heat transfer rate was obtained. Garcia et al. [39] conducted a comparative analysis to evaluate the influences of corrugated, dimpled, and wire coil-inserted tubes on the hydrothermal performance. They revealed that these modified tube geometries provide a better pressure drop as compared to the heat transfer performance. The corrugated tube as a superior geometry entails the minimum friction factor. Kareem et al. [40] carried out a comprehensive study investigating the effect of different geometry on the heat transfer performance of the tube. The outcomes demonstrated that the helical corrugated structure enlarges the contact area, and also makes a swirl effect on the flow that is an essential factor to the heat transfer enhancement. Kaood and

Based on literature [41,42], it is obvious that the heat transfer efficiency of heat exchangers is increased when corrugated tubes and NFs are combined. However, based on the authors' knowledge, the numerical investigation if the BIPVT with the corrugated absorber

Table 1
Al$_2$O$_3$ and pure water features.

	μ (kg/m.s)	k (W/ $m.K$)	$C_{p,np}$ (kJ/kg. K)	ρ (kg/ m^3)
Water	1.796×10^{-3}	0.613	4.179	997.1
Al$_2$O$_3$	–	25	0.765	3970

tube and NF coolant is novel and has not been reported in the past literature. Additionally, the intelligent soft-computing modeling of the overall exergy efficiency of such BIPVT and presenting an estimation function based on the effective parameters has not been performed up to now. The objective is the evaluation of the exergy performance of a BIPVT with corrugated absorber tube at different *Re* numbers and nanoparticle concentrations as well as developing an intelligent furcating model for the estimation of the overall exergy efficiency of the system. To this end, we conducted a three-dimensional numerical parametric analysis on a corrugated absorber tube BIPVT solar collector and examined 16 different cases based on the *Re* and nanoparticle concentration. In addition, the group method for data handling (GMDH)-type Neural Network (GMDH/NN) approach was employed for devolving a predictive function for the overall exergy efficiency. The results subsequently are presented in terms of the PV mean temperature, the useful thermal exergy, the useful electrical exergy, the thermal exergy efficiency, the electrical exergy efficiency, as well as the overall exergy efficiency of the studied BIPVT. In the final part, the results of GMDH/NN and a formulation for the estimation of the overall exergy efficiency will be presented.

2. Numerical simulations

The 3-D forced convection laminar flow model was developed and used in this work. The geometry of the BIPVT with a corrugated absorber tube is shown in Fig. 1. The studied nanofluid is a mixture with 40 nm Al$_2$O$_3$ nanoparticles suspended in water, which steadily flows in the corrugated absorber tube.

2.1. Properties of NF

The following formulations are used to determine the NF properties based on the pure water and Al$_2$O$_3$ nanoparticle properties:
The calculations for the effective thermal conductivity of NF is given as follows [,43]:

$$k_{eff} = k_w \left(4.79\varphi^2 + 2.72\varphi + 1 \right) \tag{1}$$

The following correlation was applied to calculate the dynamic viscosity of NF [44,45]:

$$\mu_{nf} = \mu_w \left(123\varphi^2 + 7.3\varphi + 1 \right) \tag{2}$$

The density of NF was computed employing the following equation [42–46]:

$$\rho_{nf} = (1 - \varphi)\rho_w + \varphi\rho_{np} \tag{3}$$

The specific heat of NF was determined employing the following equation [42–46]:

$$\rho_{nf}C_{p,nf} = (1 - \varphi)\rho_w C_{p,w} + \varphi\rho_{np}C_{p,np} \tag{4}$$

Table 1 presents the properties of Al$_2$O$_3$ nanoadditives and pure water.

2.2. Governing equations

The flow and Heat transfer are investigated using the governing equations of mass continuity, momentum, and energy, which are introduced as equations present as (5) to (8), respectively [47–49]:

$$\nabla(\rho_m.V_m) = 0 \tag{5}$$

$$\nabla.(\rho_m V_m V_m) = -\nabla p_m + \mu_m \nabla^2 V_m + \nabla.\left(\sum_{k=1}^{n} \varphi_p \rho_p V_{dr,p} V_{dr,p} \right) \tag{6}$$

$$-\nabla(\varphi_p \rho_p V_m) = -\nabla(\varphi_p \rho_p V_{dr,p}) \tag{7}$$

$$\nabla.\left(\sum_{k=1}^{n} \varphi_p \rho_p V_p C_{p,p} T_p \right) = \nabla.\left(k_{eff} \nabla T \right) \tag{8}$$

In Eq. (6), $V_{dr,p}$ is the relative velocity of the nanoparticle phase to the mixture phase and is known as the drift velocity [47–49]:

$$V_{dr,p} = \underbrace{\left(V_p - V_f \right)}_{V_{pf}:slip\ velocity} - \sum_{k=1}^{n} \frac{\varphi_p.\rho_p}{\rho_m}.\left(V_p - V_f \right) \tag{9}$$

where, p and f denote the particle and fluid phases, respectively. Also, m refers to the mixture of NF. Manninen [49] suggested the following equation for calculating the slip velocity:

$$V_{pf} = \frac{\rho_p . d_p{}^2}{18.\mu_f . f_{drag}} \frac{(\rho_p - \rho_m)}{\rho_m} . \alpha \tag{10}$$

where, α is the acceleration and given as follows:

$$\alpha = g - (V_m . \nabla) V_m \tag{11}$$

In addition, the drag velocity, which is used in Eq. (10), is given as follows [48]:

$$f_D = \begin{cases} 1 + 0.15 Re_{np}^{0.687} \rightarrow Re \leq 1000 \\ 1 + 0.15 Re_{np} \rightarrow Re > 1000 \end{cases} \tag{12}$$

2.3. Performance metrics

The comparison between different cases of Re and ω was made using four performance metrics namely a) thermal exergy efficiency (Υ_t), b) electrical exergy efficiency (Υ_e), c) overall exergy efficiency (Υ_{ov}), and d) useful thermal exergy (Ex_u) which are calculated using Eqs. (13)–(16) [50]:

$$Ex_{u,t} = \dot{m} c_p (T_{out} - T_{in}) \left[1 - \frac{T_a}{T_{mean}} \right] \tag{13}$$

$$\Upsilon_e = \frac{16.5 [1 - 0.00451 (T_{PV} - 293)] \alpha_{PV} . I_s . A_{PVT} - \frac{2\dot{m}\Delta P}{\rho}}{I_s . A_{PVT}} \tag{14}$$

$$\Upsilon_t = \frac{Ex_u}{I_s . A_{PVT} . \left(1 - \frac{4}{3} \left(\frac{T_a}{T_{sky}} \right) + \left(\frac{T_a}{T_{sky}} \right)^4 \right)} \tag{15}$$

$$\Upsilon_{ov} = \Upsilon_t + \Upsilon_e \tag{16}$$

2.4. Boundary conditions

A uniform flow at the inlet of the tube with a different velocity corresponding to $Re = 500$–2000 and an inlet temperature of 293 K was considered. The derivatives of velocity, temperature, and pressure at the outlet were set as zero. A uniform heat flux of 2.83 MW/m^3 was considered for the absorber tube body. At the wall surfaces, the non-slip condition was set and the outlet velocity was set as the ambient pressure. In the negative direction of Y, the gravity acceleration was set as 9.82 m/s^2. In addition, according to the two-phase mixture assumptions, the nanoparticle and base fluid velocities and temperatures were considered to be equal at the absorber tube inlet.

2.5. Intelligent GMDH-type neural network

Several heuristic algorithms are available for developing accurate functions based on the real input data; most of these models provide a computer-based function for prediction, and extracting the coefficients or polynomial constants is not simple [51]. Machine learning is a branch of artificial intelligence that allows machines to learn without being programmed [52,53]. Neural network is known as a kind of machine learning algorithm in which a self-organization approach is employed to heuristically build an artificial neural network [54–58]. The GMDH-type neural network is known as a kind of machine learning algorithm in which a self-organization approach is employed to heuristically build an artificial neural network. GMDH-ANN is used in prediction, data mining, forecasting, knowledge discovery, pattern identification, and modeling of different systems [59]. This inductive algorithm automatically finds the interrelations between data. The capability of the GMDH-ANN model in evaluating the neurons in the hidden layers and removing the less important parameters in each iteration leads to obtaining the optimum and accurate predictive functions. Ivakhnenko [60] introduced and presented the GMDH algorithm for the first. Sawaragi et al. [61] used the GMDH to develop an air pollution prediction model. They concluded that this method is more accurate than other time series models. GMDH separates the real data into two categories train and test data sets. For the first, the machine is trained using the training dataset and in the next stage, the developed model is tested using the remainder of the data (test data). Some input parameters would be eliminated during the search process and once, the minimum deviation between the real data and predicted data is achieved, the iteration is terminated [62]. The general polynomial, which is constructed using GMDH, is known as Kolmogorov-Gabor and is given as follows [51,59,and 63]]:

$$\hat{y} = a_0 + \sum_{i=1}^{k} a_i x_i + \sum_{i=1}^{k} \sum_{j=1}^{k} a_{ij} x_i x_j + \sum_{i=1}^{k} \sum_{j=1}^{k} \sum_{z=1}^{k} a_{ij} x_i x_j x_z + \ldots \tag{17}$$

where $\hat{y}$ is the predicted output and x_i are the inputs of model, a denote the polynomial coefficients, and k represents the number of inputs. We used the Re and nanoparticle volume fraction as inputs and the overall exergy efficiency, Υ_{ov} is the output function. A

Table 2
Results of checking the numerical method validity.

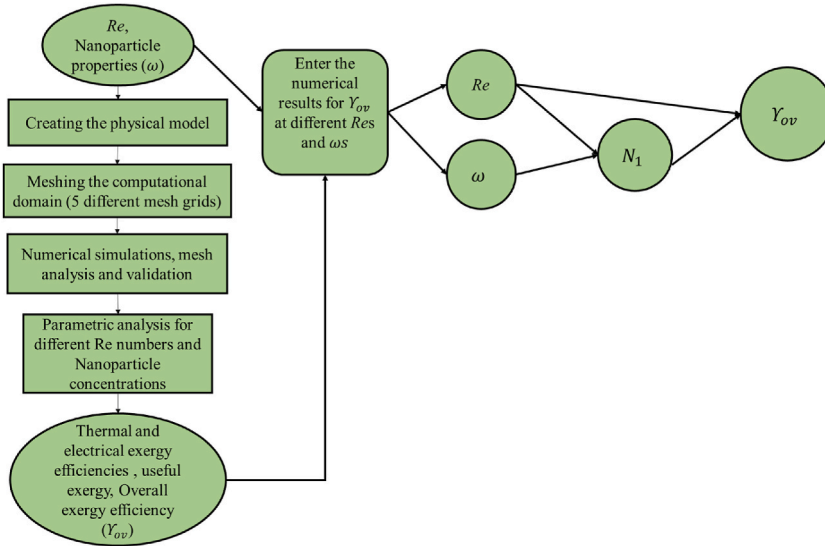| ω	Ref. [64]	Current study
0	314.098	314.321
0.5	313.976	314.183
1.0	313.862	314.043
1.5	313.678	313.875
2.0	313.563	313.743

Fig. 2. The flow chart of numerical simulation and machine learning modeling.

second-order polynomial was developed for the Υ_{ov} as follow:

$$\widehat{Z} = a_0 + a_1 Re + a_2 \omega + a_3 Re^2 + a_4 \omega^2 + a_5 Re.\omega \tag{18}$$

The above polynomial is the output of a neuron in the first hidden layer based on two input parameters (Re, ω). Then, it is used as one input data of the second layer to construct another polynomial while the other input parameter is Re:

$$\widehat{\Upsilon_{ov}} = a_0 + a_1 Re + a_2 \widehat{Z} + a_3 Re^2 + a_4 \widehat{Z}^2 + a_5 Re.\widehat{Z} \tag{19}$$

2.6. Mesh optimization

Ensuring that the numerical results do not depend on the number of grid elements is a an important issue that should be considered in all numerical research. To ensure this, six different grids were prepared, the number of elements of which were 345542, 519098, 793265, 1174903, 1794031, and 2549231. By calculating the fluid outlet temperature and inlet pressure for case $Re = 2000$ and $\omega = 1$ % using all six grids, it was found that increasing the number of elements to more than 1794031 does not affect the results and only increases the run time, which is undesirable.

2.7. Numerical model verification

Checking whether the numerical scheme employed in the current contribution has sufficient accuracy or not was done by comparing the PV panel temperature of a nanofluid-based PVT with ribbed absorber tube by Fu et al. [64] with the data obtained from the present research. The comparison results tabulated in Table 2 revealed a slight difference between the results of two studies.

3. Results and discussion

The numerical analysis was conducted using the Finite Volume Method (FVM) in the ANSYS Fluent software. The procedure of the whole modeling is illustrated in Fig. 2. As can be seen, the geometry of the PVT absorber tube is firstly created and then five grids with different numbers of node were developed to assure the independency of the numerical results to the grid size. Then the numerical results were verified using the results of the previous studies. Afterward, the parametric analysis was performed to determine different performance factors considering different Re numbers and nanoparticle concentration. The output results for the overall exergy efficiency at two input variables (Re and ω) were used in the machine learning modeling to develop a high accurate model for the estimation of the overall exergy efficiency.
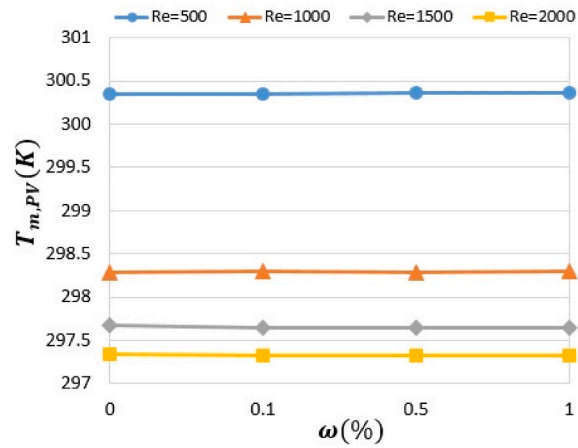
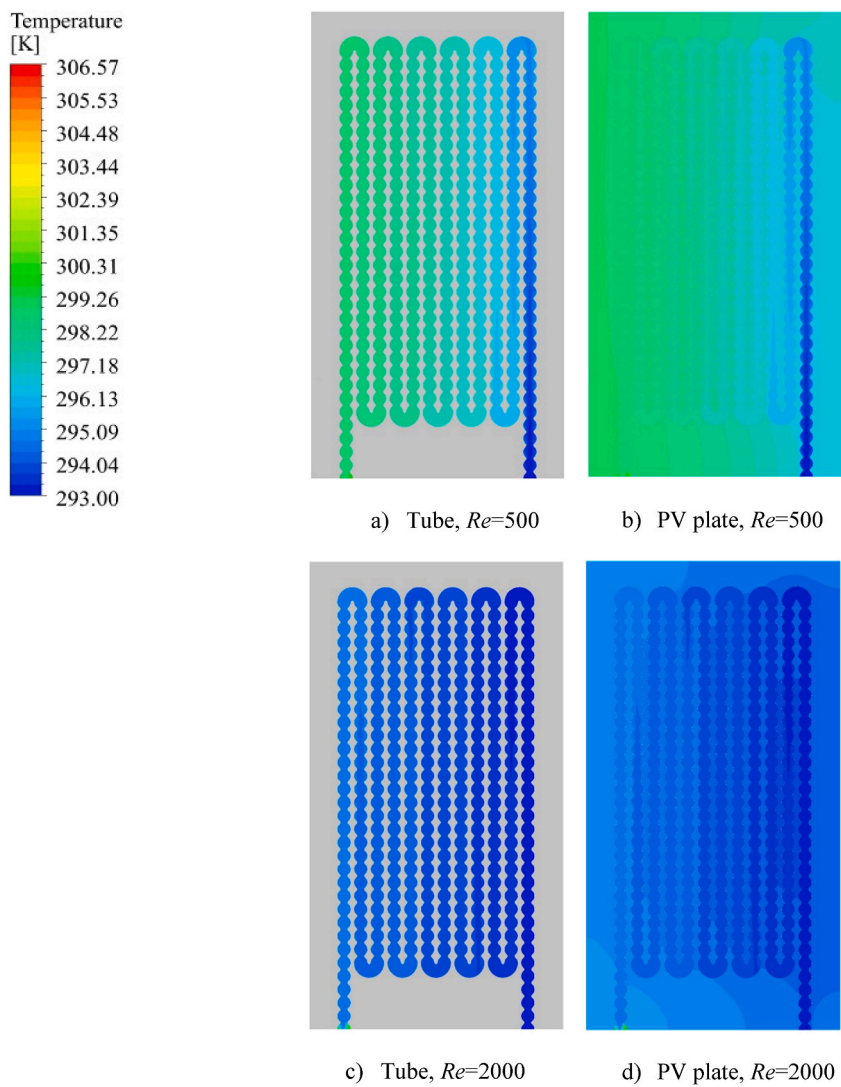**Fig. 3.** Useful thermal exergy versus *Re* number and volume fraction.

a) Tube, *Re*=500

b) PV plate, *Re*=500

c) Tube, *Re*=2000

d) PV plate, *Re*=2000

Fig. 4. The temperature contour plots for the absorber tube and PV plate for $\omega = 1$ %.
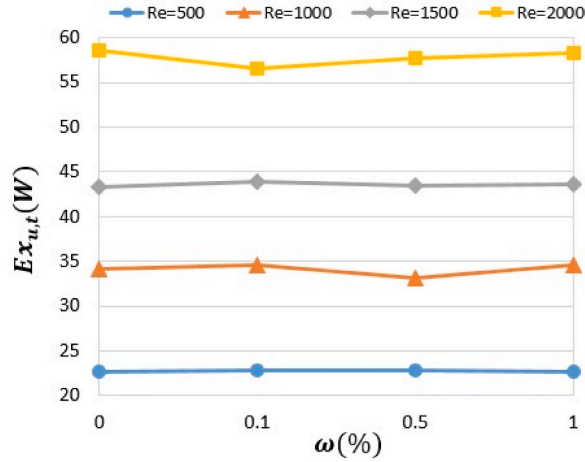
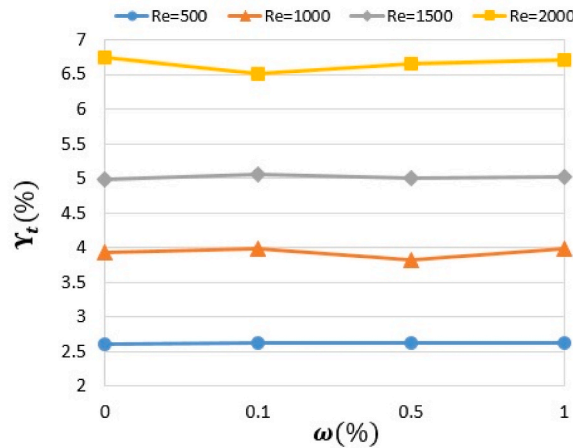**Fig. 5.** Useful thermal exergy versus *Re* number and volume fraction.

Fig. 6. Thermal exergy efficiency versus *Re* number and volume fraction.

3.1. Numerical outputs

The change in the *Re* and nanoparticle concentration both affect the hydrothermal characteristics and exergy destruction rate of the studied BIPVT. The exergy destruction is associated with the frictional or thermal irreversibilities that might happen as the result of a change in flow velocity and other specifications. The influence of intensification of nanoparticle volume fraction (ω) and *Re* number on the mean temperature of the BIPVT is illustrated in Fig. 3. The prominent effect of *Re* against ω is evident in this figure. Nearly 1.014 % and 1.023 % reduction in $T_{m,PV}$ is observed as *Re* goes up from 500 to 2000 considering ω s of 0 % and 1 %, respectively. Nanoparticle concentration increment, however, with a maximum of 0.0089 % in $T_{m,PV}$ has no significant effect on the PV mean temperature.

The temperature contour plots for the absorber tube and PV plate are shown in Fig. 4. Since, the nanoparticle concentration has a low impact on the temperature distribution, the contour plots are shown for the constant ω of 1 % and two Re numbers 500 and 2000. As can be seen from Fig. 4a and c, the inlet region has lower temperature distribution due to the lower NF temperature and the temperature arises as NF flows inside the tube. The higher heat is transferred from the PV plate to the NF, thereby the NF temperature at the exit of the collector is high. The comparison between Fig. 4b and d discloses that the increase in *Re* leads to enhancing the flow mixing and heat transfer rate, thereby the PV plate temperature reduces. It is worth mentioning that the escalation of *Re* leads to increasing the NF mass flow rate, thereby the NF temperature at the outlet of the absorber tube at *Re* = 2000 is lower than that at *Re* = 500.

Fig. 5 shows the useful thermal exergy of the BIPVT at different *Re* numbers and ω s. It is evident that the *Re* increment improves $Ex_{u,t}$; nearly 60 % enhancement is observed as *Re* increases from 500 to 2000 regardless of ω magnitude. The reason is that the flow mixing and convective heat transfer coefficient enhance as *Re* escalates, thereby a greater part of the input exergy of the sun is extracted by the corrugated absorber tube. Nevertheless, the highest percentage improvement in $Ex_{u,t}$ by changing ω is obtained as 0.69 %, 4.19 %, 1.36 %, and 3.24 %, respectively, at *Re*s 500, 1000, 1500, 2000. Besides, the highest values of $Ex_{u,t}$ is obtained at ω s of
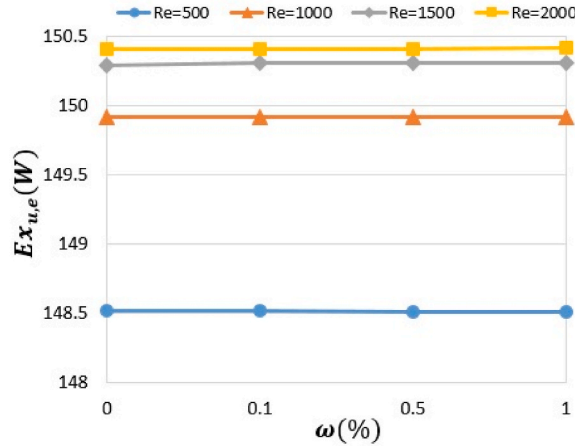
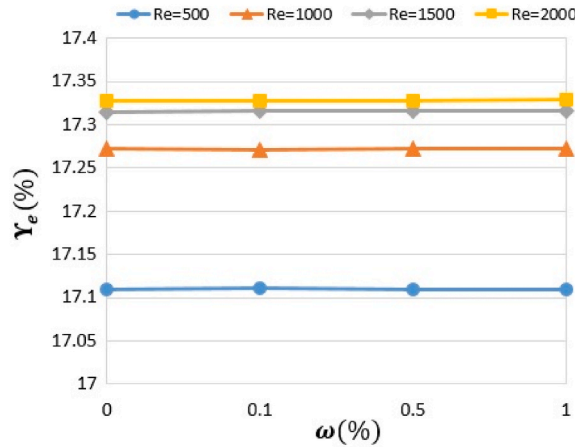**Fig. 7.** Useful electrical exergy versus *Re* number and volume fraction.

Fig. 8. Electrical exergy efficiency versus *Re* number and volume fraction.

0.1 % for *Re*s 1000 to 1500 and at $\omega = 0$ % for $Re = 2000$. A similar trend occurs for thermal exergy efficiency of BIPVT, Υ_t (Fig. 6). The lowest and highest Υ_t s were determined as 2.60 % and 6.73 %, respectively, at *Re*s 500 and 2000 and $\omega = 0$ %. It is worth noting that for $Re = 2000$, nearly the same Υ_t vales are obtained at $\omega = 0$ % and $\omega = 1$ % (6.73 % and 6.70 %). The increase in nanoparticle concentration increases the nanofluid density and dynamic viscosity at different paces. Thereby, based on the *Re* formulation, the dominant increasing rate of density over the dynamic viscosity leads to decreasing velocity and vice versa to maintain a constant *Re*. Therefore, the increasing-decreasing trends of Υ_t and $Ex_{u,t}$ with the escalation of ω depending on the increase or decrease in the NF velocity. Fig. 5 also discloses that the low value of Υ_t is due to the huge exergy destruction of the BIPVTs against the concentrated solar collectors. The input exergy of the sun is high per square meter of the PVT and only 2.6–6.73 % of this exergy is captured by the system.

The useful electricity is equal to the output electricity of PVT minus the required pumping power of the NF. Fig. 7 shows the improvement in $Ex_{u,e}$ with the increment in *Re* number and ω. As can be seen, an average value of 149.5 W for the $Ex_{u,e}$ is obtained within the studied *Re* range. Meanwhile, the variations trend of $Ex_{u,e}$ with ω is not significant; highest increase is 0.0114 %. In addition, nearly 1.256%–1.267 % improvement in $Ex_{u,e}$ is obtained for ω s of 0%–1% as *Re* surges up from 500 to 2000. The cooling performance of the BIPVT determines its electrical efficiency; the higher the PV panel is, the greater $Ex_{u,e}$ will be. The intensification of *Re* means a better flow mixing has occurred inside the corrugated absorber tube leading to heat transfer rate enhancement and thereby lower temperature of the PV plate. In consequence, the useful electrical exergy and efficiency electrical exergy efficiency are improved as can be seen in Figs. 7 and 8.

The velocity contour plots at two Re numbers 500 and 2000 and ω values of 0 % and 1 % are show in Fig. 9. As can be seen, the effect of increasing the nanoparticle concentration is bolder in the low Re of 500, so that the areas with the red color at the core of the tube is higher for $\omega = 1$ % (Fig. 9b) as compared to that for $\omega = 0$ % in Fig/9a. In addition, the escalation in Re significantly increases the velocity distribution inside the tube as can be seen from Fig. 9c and d.

The overall exergy efficiency variations trend obeys that of the useful thermal exergy and thermal exergy efficiency since Υ_{ov} is the summation of Υ_t and Υ_e based on Eq. (16). As observed in Fig. 10, Υ_{ov} changes from 19.70 % to 24.06 % by increase in *Re* and ω.

a) Re=500, ω=0%   b) Re=500, ω=1%

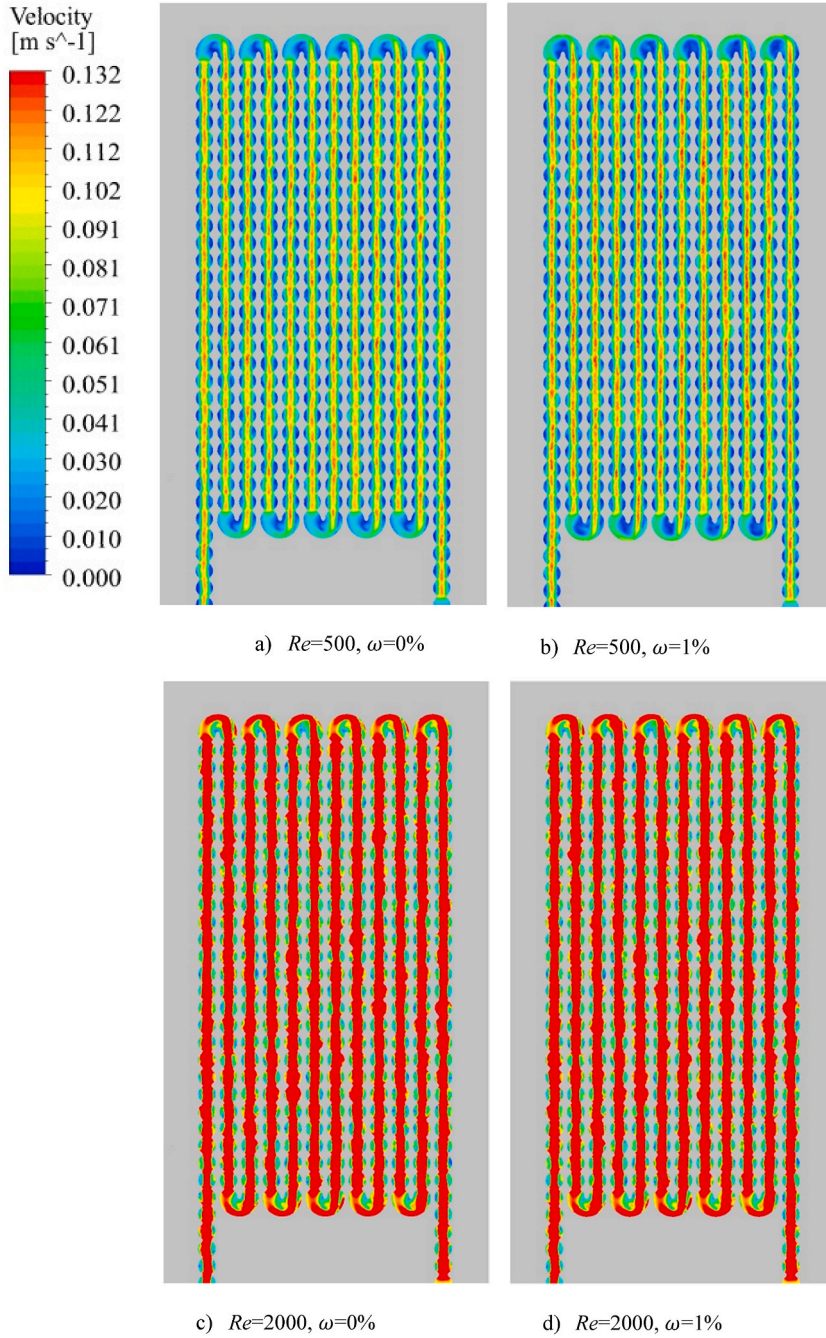c) Re=2000, ω=0%   d) Re=2000, ω=1%

Fig. 9. The velocity contour plots inside the absorber tube.

Besides, the escalation of Re from 500 to 2000 improves Υ_{ov} by almost 17.5 % at different volume concentrations of NF. The highest and lowest enhancement in Υ_{ov}, which are obtained due to increment in ω from 0 % to 1 %, are equal to 0.095 % and 0.909 % at Re numbers of 500 and 2000, respectively.

3.2. Intelligent forecasting results

Performance analysis of the GMDH network is presented in this part. As mentioned earlier, 2 input parameters of Re and ω were used to develop a second-order Kolmogorove-Gabor predictive polynomial. This number is also used as the maximum number of neurons per layer. Totally 16 data points were used; 10 points of which were applied as the test samples and 6 points were used as the train samples. The resultant polynomial (N_1) and the Re number were used to determine the final second-order polynomial. The first function (N_1) and the final developed function for estimating $\widehat{\Upsilon}_{ov}$ are presented in **Eq. (20)** and **(21)**, respectively.
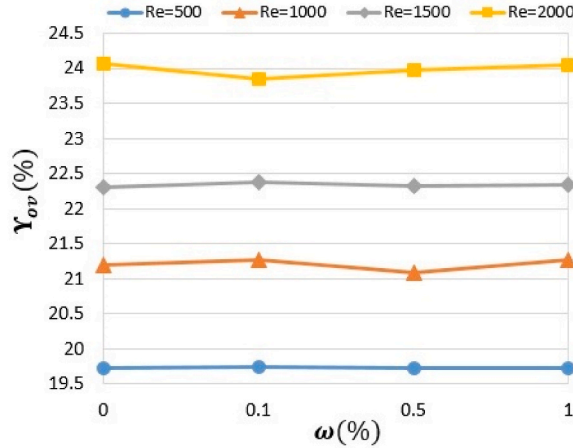
Fig. 10. Overall exergy efficiency versus *Re* number and volume fraction.
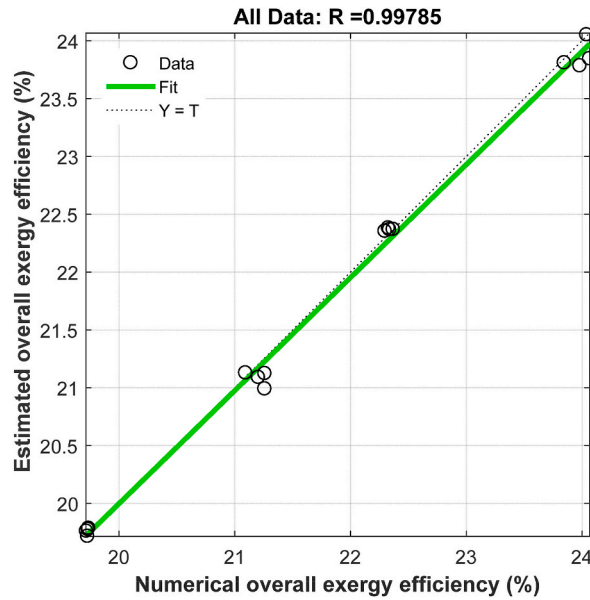

Fig. 11. The scatter plot and coefficient of determination.

$$N_1 = 18.6268563270657 - 0.247980016336783 \times \omega + 0.00215323029207107 \times Re$$

$$+0.504775816608735 \times \omega^2 + 2.69955956015219E - 07 \times Re^2 - -0.0000649701957268385 \times \omega \times Re \qquad (20)$$

$$\Upsilon_{ov} = 1207.97122286723 - 127.883730214407 \times N_1 + 0.337265284958974 \times Re - 3.43714533900072 \times N_1^2$$

$$+0.0000236698185260452 \times Re^2 - 0.0179986950521627 \times N_1 \times Re$$

GMDH results are illustrated in Figs. 11 and 12 for all 16 points based on the coefficient of determination scatter plot and error plots. As observed, with $R^2 = 0.99785$ and MAE and RMAE of 0.013 and 0.114, respectively, there is a very good agreement of input numerical data and predicted outputs indicating that the GMDH network is suitably able to capture the overall exergy efficiency.

4. Conclusion

We performed a numerical analysis on the forced convection laminar flow (Re = 500–2000) of Al_2O_3/water nanofluid as the coolant in a corrugated absorber tube of a BIPVT solar collector. The nanoparticle volume fractions (ω) and Re were changed to investigate the influence of these two important parameters on useful thermal and electrical exergies as well as exergy efficiencies. The effect of *Re* was prominent as compared to ω. So, the escalation in *Re* from 500 to 2000 intensified pumping power by 94 % and reduced
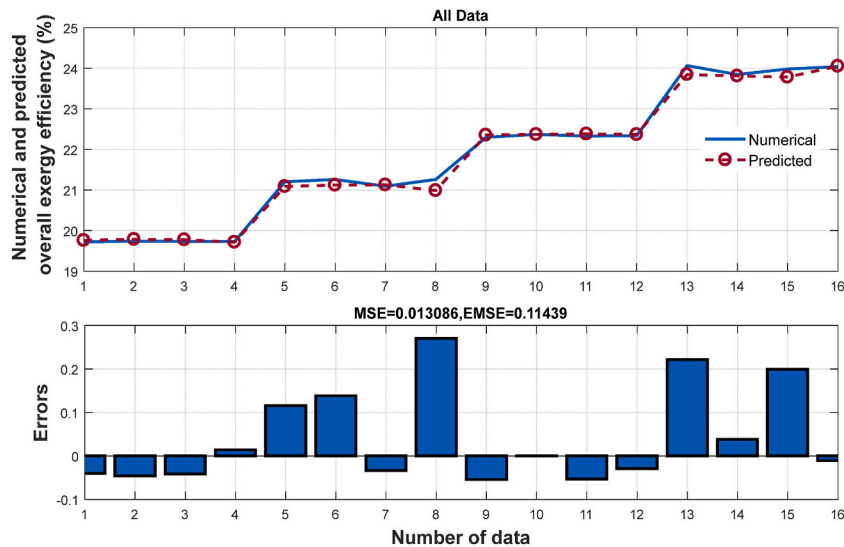
Fig. 12. GMDH performance metrics for the BIPVT overall exergy efficiency.

the PV mean temperature by 1 %. In addition, the useful thermal exergy (thermal exergy efficiency) and electrical exergy (and electrical exergy efficiency) enhanced by 60 % and 1.26 %, respectively, for the mentioned increment in Re. While a 17 % improvement in the overall exergy efficiency was observed for Re escalation from 500 to 2000. On the other hand, the effect of ω is insignificant and with the escalation of ω from 0 % to 1 %, the useful thermal exergy and thermal exergy efficiency improved by 0.39 %, 1.39 %, and 0.74 %, respectively, at Res of 500, 1000, and 1500, and reduced by 0.39 % for Re = 2000. Moreover, the minimum and maximum values of overall exergy efficiency (19.71 % and 24.06 %) were obtained at Re numbers 500 and 2000, respectively. The results of the GMDH-type ANN soft-computing method showed that the estimated values of overall exergy efficiency have an insignificant deviation from the numerical values (having $R^2 = 0.9953$ and MSE = 0.013806) indicating the high capability of the model in prediction of this performance parameter.

Author statement

Chuan Sun: Methodology, Software and Validation, Investigation, Revision. **Mohammad Naser Fares:** Methodology, Software and Validation, Investigation, Revision. **S. Mohammad Sajadi:** Methodology, Software and Validation, Revision. **Z Li:** Methodology, Software and Validation, Writing - Original Draft; Investigation, Revision. **Dheyaa J. Jasim:** Methodology, Software and Validation, Writing - Original Draft; Investigation. **Karrar A. Hammoodi:** Methodology, Software and Validation, Writing - Original Draft; Investigation. **Navid Nasajpour-Esfahani:** Methodology, Software and Validation, Writing - Original Draft; Investigation. **Soheil Salahshour:** Methodology, Software and Validation, Investigation, Revision. **As'ad Alizadeh:** Investigation, Revision.

Declaration of competing interest

The authors declare that they have no known competing financial interests or personal relationships that could have appeared to influence the work reported in this paper.

Data availability

No data was used for the research described in the article.

Acknowledgement

References

[1] Li, R., Xu, D., Tian, H., & Zhu, Y. (2023). Multi-objective study and optimization of a solar-boosted geothermal flash cycle integrated into an innovative combined power and desalinated water production process: Application of a case study. Energy, 282, 128706. doi: https://doi.org/10.1016/j.energy.2023.128706.

[2] Zhang, L., Wang, Y., Ding, B., Gu, J., Ukrainczyk, N.,... Cai, J. (2023). Development of geopolymer-based composites for geothermal energy applications. Journal of Cleaner Production, 419, 138202. doi: https://doi.org/10.1016/j.jclepro.2023.138202.

[3] M. Shakouri, H. Ebadi, Sh Gorjian, Chapter 4 - Solar Photovoltaic Thermal (PVT) Module Technologies. Photovoltaic Solar Energy Conversion, Academic Press, 2020, pp. 79–116.

[4] M. Karami, M. Jalalizadeh, Performance comparison and risk assessment of BIPVT-based trigeneration systems using vapor compression and absorption chillers, J. Build. Eng. 69 (2023), 106244.

[5] M. Jalalizadeh, R. Fayaz, Sh Delfani, H.J. Mosleh, M. Karami, Dynamic simulation of a trigeneration system using an absorption cooling system and building integrated photovoltaic thermal solar collectors, J. Build. Eng. 43 (2021), 102482.

[6] S. Bae, H. Chae, Y. Nam, Experimental analysis of an integrated system using photovoltaic–thermal and air source heat pump for real applications, Renew. Energy 217 (2023), 119128.

[7] H. Gh Ahsaee, I.B. Askari, The application of thermoelectric and ejector in a CO2 direct-expansion ground source heat pump; energy and exergy analysis, Energy Convers. Manag. 226 (2020), 113526.

[8] H.M. Maghrabie, K. Elsaid, E.T. Sayed, M.A. Abdelkareem, T. Wilberforce, A.G. Olabi, Building-integrated photovoltaic/thermal (BIPVT) systems: applications and challenges, Sustain. Energy Technol. Assessments 45 (2021), 101151.

[9] K. Terashima, H. Sato, T. Ikaga, PV/T solar panel for supplying residential demands of heating/cooling and hot water with a lower environmental thermal load, Energy Build. 297 (2023), 113408.

[10] A. Zarei, S. Akhavan, M. Ghodrat, M. Behnia, Thermodynamic analysis and multi-objective optimization of a modified solar trigeneration system for cooling, heating and power using photovoltaic-thermal and flat plate collectors, Int. Commun. Heat Mass Tran. 137 (2022), 106261.

[11] A. Zarei, S. Akhavan, M.B. Rabiee, S. Elahi, Energy, exergy and economic analysis of a novel solar driven CCHP system powered by organic Rankine cycle and photovoltaic thermal collector, Appl. Therm. Eng. 194 (2021), 117091.

[12] I.B. Askari, F. Calise, M. Vicidomini, Design and comparative techno-economic analysis of two solar polygeneration systems applied for electricity, cooling and fresh water production, Energies 12 (22) (2019) 4401.

[13] M.H. Jahangir, S.M.E. Razavi, A. Kasaeian, H. Sarrafha, Comparative study on thermal performance of an air based photovoltaic/thermal system integrated with different phase change materials, Sol. Energy 208 (2020) 1078–1089.

[14] A. Shahsavar, M. Jafari, I. Baniasad Askari, F. Selimefendigil, Thermo-hydraulic performance and entropy generation of biologically synthesized silver/water-ethylene glycol nano-fluid flow inside a rifled tube using two-phase mixture model, Energy Sources, Part A Recovery, Util. Environ. Eff. (2020), https://doi.org/10.1080/15567036.2020.1850932.

[15] I.B. Mansir, R. Chaturvedi, Z. Abubakar, D.U. Lawal, J.A. Yusuf, Numerical investigation of the effect of cross-section on the hydrothermal and irreversibility features of water/Fe3O4 ferrofluid flow inside a twisted tube in the presence of an external magnetic field effect Engineering Analysis with Boundary, Elements 157 (2023) 119–135, https://doi.org/10.1016/j.enganabound.2023.08.039.

[16] A. Kumar, R. Maithani, M. Ashraf Ali, N.K. Gupta, S. Sharma, T. Alam, H. Sh Majdi, T.M.Y. Khan, A.S. Yadav, S.M. Eldin, Enhancement of heat transfer utilizing small height twisted tape flat plate solar heat collector: a numerical study, Case Stud. Therm. Eng. 48 (2023), 103123, https://doi.org/10.1016/j.csite.2023.103123.

[17] Q. Gong, Ch Yu, W. Wang, Y. Wang, Experimental and numerical exploration on improved heat transfer by continuous spiral flow in shell of spiral wound corrugated tube heat exchanger, Case Stud. Therm. Eng. 51 (2023), 103483, https://doi.org/10.1016/j.csite.2023.103483.

[18] G. Wang, C. Qi, M. Liu, Ch Li, Y. Yan, L. Liang, Effect of corrugation pitch on thermo-hydraulic performance of nanofluids in corrugated tubes of heat exchanger system based on exergy efficiency, Energy Convers. Manag. 186 (2019) 51–65.

[19] H. Wei, H. Moria, K.S. Nisar, R. Ghandour, A. Issakhov, Y.L. Sun, A. Kaood, M.M. Youshanlouei, Effect of volume fraction and size of Al2O3 nanoparticles in thermal, frictional and economic performance of circumferential corrugated helical tube, Case Stud. Therm. Eng. 25 (2021), 100948.

[20] R.M.I. Islam, N.M.S. Hassan, M.G. Rasul, P.V. Gudimetla, M.N. Nabi, A.A. Chowdhury, Effect of non-uniform wall corrugations on laminar convective heat transfer through rectangular corrugated tube by using graphene nanoplatelets/MWCN hybrid nanofluid, Int. J. Therm. Sci. 187 (2023), 108166, https://doi.org/10.1016/j.ijthermalsci.2023.108166.

[21] D. Zheng, J. Du, W. Wang, J.J. Klemeš, J. Wang, B. Sundén, Analysis of thermal efficiency of a corrugated double-tube heat exchanger with nanofluids, Energy 256 (2022), 124522.

[22] C. Qi, Y.L. Wan, C.Y. Li, D.T. Han, Z.H. Rao, Experimental and numerical research on the flow and heat transfer characteristics of TiO2-water nanofluids in a corrugated tube, Int. J. Heat Mass Tran. 115 (2017) 1072–1084.

[23] A. Shahsavar, S. Entezari, I. Baniasad Askari, M. Jamei, M. Karbasi, M. Shahmohammadi, Investigation on two-phase fluid mixture flow, heat transfer and entropy generation of a non-Newtonian water-CMC/CuO nanofluid inside a twisted tube with variable twist pitch: numerical and evolutionary machine learning simulation, Eng. Anal. Bound. Elem. 140 (2022) 322–337, https://doi.org/10.1016/j.enganabound.2022.04.022.

[24] M. Bahiraei, N. Mazaheri, M. Hanooni, Performance enhancement of a triple-tube heat exchanger through heat transfer intensification using novel crimped-spiral ribs and nanofluid: a two-phase analysis, Chemical Engineering and Processing - Process Intensification 160 (2021), 108289.

[25] M.S. Shuvo, T.H. Ruvo, S. Saha, Characteristics of turbulent forced convective nanofluid flow and heat transfer in a 2D axisymmetric corrugated pipe, Therm. Sci. Eng. Prog. 41 (2023), 101838.

[26] M. Khan, I.N. Alsaduni, M. Alluhaidan, W.F. Xia, M. Ibrahim, Evaluating the energy efficiency of a parabolic trough solar collector filled with a hybrid nanofluid by utilizing double fluid system and a novel corrugated absorber tube, J. Taiwan Inst. Chem. Eng. 124 (2021) 150–161, https://doi.org/10.1016/j.jtice.2021.04.045.

[27] R.K. Ajeel, W.S. Islam, K. Sopian, M.Z. Yusoff, Analysis of thermal-hydraulic performance and flow structures of nanofluids across various corrugated channels: an experimental and numerical study, Therm. Sci. Eng. Prog. 19 (2020), 100604.

[28] D. Wang, M.A. Ali, K. Sharma, S.F. Almojil, A. Alizadeh, A.F. Alali, A.I. Almohana, Multiphase numerical simulation of exergy loss and thermo-hydraulic behavior with environmental cosiderations of a hybrid nanofluid in a shell-and-tube heat exchanger with twisted tape, Eng. Anal. Bound. Elem. 147 (2023) 1–10.

[29] H. Maddah, R. Aghayari, M. Mirzaee, M.H. Ahmadi, M. Sadeghzadeh, A.J. Chamkha, Factorial experimental design for the thermal performance of a double pipe heat exchanger using Al2O3-TiO2 hybrid nanofluid, Int. Commun. Heat Mass Tran. 97 (2018) 92–102.

[30] C. Qi, G. Wang, Y. Yan, S. Mei, T. Luo, Effect of rotating twisted tape on thermo-hydraulic performances of nanofluids in heat-exchanger systems, Energy Convers. Manag. 166 (2018) 744–757.

[31] P. Naphon, Experimental investigation the nanofluids heat transfer characteristics in horizontal spirally coiled tubes, Int. J. Heat Mass Tran. 93 (2016) 293–300.

[32] X. Zhai, C. Qi, Y. Pan, T. Luo, L. Liang, Effects of screw pitches and rotation angles on flow and heat transfer characteristics of nanofluids in spiral tubes, Int. J. Heat Mass Tran. 130 (2019) 989–1003.

[33] M. Akbarzadeh, S. Rashidi, M. Bovand, R. Ellahi, A sensitivity analysis on thermal and pumping power for the flow of nanofluid inside a wavy channel, J. Mol. Liq. 220 (2016) 1–13.

[34] A.A.R. Darzi, M. Abuzadeh, M. Omidi, Numerical investigation on thermal performance of coiled tube with helical corrugated wall, Int. J. Therm. Sci. 161 (2021), 106759.

[35] Sanaz Akbarzadeh, Mohammad Sadegh Valipour, Energy and exergy analysis of a parabolic trough collector using helically corrugated absorber tube, Renew. Energy 155 (2020) 735–747.

[36] M.R. Esfahani, E.M. Languri, Exergy analysis of a shell-and-tube heat exchanger using graphene oxide nanofluids, Exp. Therm. Fluid Sci. 83 (2017) 100–106.

[37] H. Chen, H. Moria, Saba Y. Ahmed, K.S. Nisar, A.M. Mohamed, B. Heidarshenas, A. Arsalanloo, M.M. Youshanlouei, Thermal/exergy and economic efficiency analysis of circumferentially corrugated helical tube with constant wall temperature, Case Stud. Therm. Eng. 23 (2021), 100803.

[38] S. Mei, C. Qi, T. Luo, X. Zhai, Y. Yan, Effects of magnetic field on thermo-hydraulic performance of Fe3O4-water nanofluids in a corrugated tube, Int. J. Heat Mass Tran. 128 (2019) 24–45.

[39] A. García, J.P. Solano, P.G. Vicente, A. Viedma, The influence of artificial roughness shape on heat transfer enhancement: corrugated tubes, dimpled tubes and wire coils, Appl. Therm. Eng. 35 (2012) 196–201.

[40] Z.S. Kareem, M.N. Mohd Jaafar, T.M. Lazim, S. Abdullah, A.F. AbdulWahid, Heat transfer enhancement in two-start spirally corrugated tube, Alex. Eng. J. 54 (2015) 415–422.

[41] A. Shahsavar, A. Godini, P.T. Sardari, et al., Impact of variable fluid properties on forced convection of Fe_3O_4/CNT/water hybrid nanofluid in a double-pipe mini-channel heat exchanger, J Therm Anal Calorim 137 (2019) 1031–1043. https://doi.org/10.1007/s10973-018-07997-6.

[42] E. Khodabandeh, R. Boushehri, O.A. Akbari, et al., Numerical investigation of heat and mass transfer of water—silver nanofluid in a spiral heat exchanger using a two-phase mixture method, J Therm Anal Calorim 144 (2021) 1003–1012. https://doi.org/10.1007/s10973-020-09533-x.

[43] M. Keshavarz Moraveji, E. Esmaeili, Comparison between single-phase and two-phases CFD modeling of laminar forced convection flow of nanofluids in a circular tube under constant heat flux, Int. Commun. Heat Mass Tran. 39 (2012) 1297–1302.

[44] M. Bahiraei, S.I. Vasefi, A novel thermal dispersion model to improve prediction of nanofluid convective heat transfer, Adv. Powder Technol. 25 (2014) 1772–1779.

[45] M.S. Mojarrad, A. Keshavarz, A. Shokouhi, Nanofluids thermal behavior analysis using a new dispersion model along with single-phase, Heat Mass Tran. 49 (2013) 1333–1343.

[46] A. Mokmeli, M. Saffar-Avval, Prediction of nanofluid convective heat transfer using the dispersion model, Int. J. Therm. Sci. 49 (2010) 471–478.

[47] R. Lotfi, Y. Saboohi, A.M. Rashidi, Numerical study of forced convective heat transfer of nanofluids: comparison of different approaches, Int. Commun. Heat Mass Tran. 37 (2010) 74–78.

[48] M. Akbari, N. Galanis, A. Behzadmehr, Comparative analysis of single and two phase models for CFD studies of nanofluid heat transfer, Int. J. Therm. Sci. 50 (2011) 1343–1354.

[49] M. Manninen, V. Taivassalo, S. Kallio, On the Mixture Model for Multiphase Flow, Technical Res. Centre Finland Finland, 1996.

[50] A. Tiwari, M.S. Sodha, Performance evaluation of solar PV/T system: an experimental validation, Sol. Energy 80 (2006) 751–759.

[51] A.G. Ivakhnenko, Polynomial theory of complex systems, IEEE Trans. Sys. Man Cybern 4 (1971), 364e378.

[52] Y. Guo, Z. Mustafaoglu, D. Koundal, Spam Detection Using Bidirectional Transformers and Machine Learning Classifier Algorithms, Journal of Computational and Cognitive Engineering (2022). https://doi.org/10.47852/bonviewJCCE2202192.

[53] C. Hebbi, H.R. Mamatha, Comprehensive dataset building and recognition of isolated handwritten kannada characters using machine learning models, Artificial Intelligence and Applicatons (2023). https://doi.org/10.47852/bonviewAIA3202624.

[54] Z. Chen, Research on Internet Security Situation Awareness Prediction Technology based on Improved RBF Neural Network Algorithm, Journal of Computational and Cognitive Engineering (2022). https://doi.org/10.47852/bonviewJCCE149145205514.

[55] B. Yang, et al., Enhancing direct-path relative transfer function using deep neural network for robust sound source localization, CAAI Trans. Intell. Technol. 7 (3) (2022) 446–454. https://doi.org/10.1049/cit2.12024.

[56] B. Fan, et al., Intelligent vehicle lateral control based on radial basis function neural network sliding mode controller, CAAI Trans. Intell. Technol. 7 (3) (2022) 455–468. https://doi.org/10.1049/cit2.12075.

[57] L. Ma, et al., Apple grading method based on neural network with ordered partitions and evidential ensemble learning, CAAI Trans. Intell. Technol. 7 (4) (2022) 561–569. https://doi.org/10.1049/cit2.12140.

[58] P. Preethi, H.R. Mamatha, Region-based convolutional neural network for segmenting text in epigraphical images, Artificial Intelligence and applications 1 (2) 119–27. https://doi.org/10.47852/bonviewAIA2202293.

[59] S.J. Farlow, The GMDH algorithm of ivakhnenko, Am. Statistician 35 (1981), 210e215.

[60] A.G. Ivakhnenko, G.I. Krotov, N. Ivakhnenko, Theoretical Systems Ecology: Advances and Case Studies, 1970.

[61] Y. Sawaragi, T. Soeda, H. Tamura, T. Yoshimura, S. Ohe, Y. Chujo, H. Ishihara, Automatica 15 (1979) 441.

[62] M.I. Radaideh, T. Kozlowski, Analyzing nuclear reactor simulation data and uncertainty with the group method of data handling, Nucl. Eng. Technol. 52 (2020) 287–295.

[63] A.G. Ivakhnenko, The group method of data of handling; a rival of the method of stochastic approximation, Soviet Automatic Control 13 (1968) 43–55.

[64] X. Fu, M.A. El-Rahman, A.N. Abdalla, E.H. Malekshah, M. Sharifpur, The numerical analysis and optimization of a photovoltaic thermal collector with three different plain, ribbed, and porous-ribbed absorber tubes and a nanofluid coolant using two-phase model, J. Taiwan Inst. Chem. Eng. 148 (2023), 104725.